Acidic Region Tyrosines Provide Access Points for Allosteric Activation of the Autoinhibited Vav1 Dbl Homology Domain†

Gaya K. Amarasinghe and Michael K. Rosen*

Howard Hughes Medical Institute and Department of Biochemistry, UT Southwestern Medical Center, 5323 Harry Hines Boulevard, Dallas, Texas 75390-8816

Received June 13, 2005; Revised Manuscript Received September 19, 2005

ABSTRACT: Autoinhibited proteins serve key roles in many signal transduction pathways, and therefore proper regulation of these proteins is critical for normal cellular function. Proto-oncogene Vav1 is an autoinhibited guanine nucleotide exchange factor (GEF) for Rho family GTPases. The core autoinhibitory module of Vav1 consists of the catalytic Dbl homology (DH) domain bound through its active site to an alpha helix centered about Tyr174 in the Acidic (Ac) region of the protein. Phosphorylation of Tyr174 and two other tyrosines in the Ac region, Tyr142 and Tyr160, relieves autoinhibition and activates the catalytic DH domain. In this study, we use biochemical and structural analyses of the Vav1 Ac and DH domains to examine the kinetic and thermodynamic properties of Vav1 activation by the Src family kinase, Lck, and the role of the Lck SH2 domain in this process. We find that in the Ac-DH fragment of Vav1, Tyr174, but not Tyr142 or Tyr160, is protected from phosphorylation by interactions with the DH domain. Binding of the Lck SH2 domain to phosphorylated Tyr142 increases k_{cat}/K_M for Tyr174 by 4-fold, likely because the kinase domain can act on the substrate effectively in an intramolecular fashion. These studies of the autoinhibited Ac-DH module provide the foundation for a quantitative structural and thermodynamic understanding of the regulation of full length Vav1. Moreover, kinetic pathways involving initial interactions with exposed sites or "access points", as observed here for Vav1, may be generally important in the regulation of many autoinhibited proteins.

Autoinhibition is a common regulatory mechanism observed in signaling proteins that control diverse processes such as cell differentiation, cell motility, and cytoskeletal rearrangement (*1*). In autoinhibited proteins, the activity of a functional domain is controlled by intramolecular interactions with a regulatory domain through either steric and/or conformational occlusion (*2*, *3*). Frequently, the thermodynamics and/or kinetics of this core autoregulatory element are further modulated through cooperative interactions of additional domains in the protein (*2*). Relief of autoinhibition requires either the physical displacement of the regulatory element or conformational changes within the regulatory and functional domains (*1*, *4*). Covalent modification of the regulatory domain or binding of an allosteric activator to it are two common mechanisms that can relieve autoinhibition. Such modifications often occur in concert with changes to other cooperatively acting elements, and must provide the energy required to disrupt autoinhibitory interactions and stimulate protein activity. Truncations of, or mutations within, the regulatory domain can disrupt the inhibitory intramolecular interactions resulting in a constitutively active functional domain (*3*). Therefore, many autoinhibited proteins are also known proto-oncogene products whose aberrant functions lead to cellular transformation, tumor invasion, and metastasis (*1*).

Many autoinhibited systems exhibit rapid activation kinetics in response to covalent modifications or activator binding to the regulatory domain (*5*). To promote activity, regulatory molecules must often access sites that are buried in the ground state of the inhibited systems (*6*−*8*). Therefore, they must either promote conformational changes that expose these sites or act on a less-populated excited state where the interaction sites are more accessible. In general, the kinetic and thermodynamic mechanisms of such activation processes are not well understood.

The guanine nucleotide exchange factor (GEF[1]) Vav1 is an autoinhibited enzyme that plays a central role in the signal transmission mediated by cell surface receptors, including the T cell, B cell, and Fcγ receptors (*9*−*12*). Vav1 and its homologues, Vav2 and Vav3, function as GEFs for Cdc42, Rac1, and RhoA, each with varying specificity (*13*, *14*). All three Vav homologues are multidomain modular proteins containing a calponin homology (CH, residues 1−134) domain, an acidic region (Ac, residues 138−190), a Dbl homology (DH, residues 191−375) domain, a pleckstrin homology (PH, residues 398−498) domain, a cysteine-rich domain (CRD, residues 506 to 570), and an SH3-SH2-SH3 module (residues 584−845) (*11*, *12*). Nucleotide

† This work was supported by a grant to M.K.R. from the NIH (GM066930). G.K.A. was supported by a postdoctoral fellowship from the Cancer Research Institute.

* Corresponding author. Phone: (214) 645-6361. Fax: (214) 645-6291. E-mail: mrosen@biochem.swmed.edu.

[1] Abbreviations: Ac, acidic region; CH, calponin homology; CRD, cysteine rich domain; DH, Dbl homology; GEF, guanine nucleotide exchange factor; ITC, isothermal titration calorimetry; Lck, lymphocyte-specific protein tyrosine kinase; NADH, nicotinamide adenine dinucleotide; NMR, nuclear magnetic resonance; PH, pleckstrin homology; PEP, phosphoenolpyruvate; PK, pyruvate kinase; SH2, Src homology 2; SH3, Src homology 3.

10.1021/bi051126h CCC: $30.25
Published on Web 10/25/2005

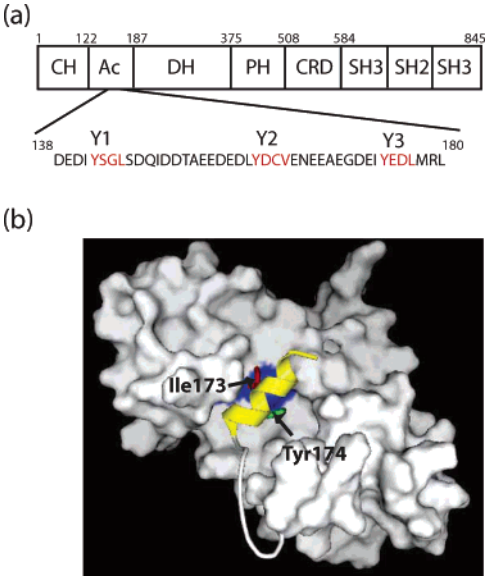

FIGURE 1: Structural domains of Vav1. (a) Structural domains of full length Vav1 and the amino acid sequence of the acidic domain. The following are labeled: CH, calponin homology domain; Ac, acidic domain; DH, Dbl homology domain; PH, pleckstrin homology domain; CRD, cysteine rich domain (also known as the zinc finger motif); SH3, Src homology 3 domain; SH2, Src homology 2 domain. Potential SH2 recognition sequences within the Ac domain are colored red. (b) Structure of the minimal autoinhibited Vav1, Y3-DH (PDB 1F5X). DH domain is shown as a white molecular surface. The Y3 inhibitory motif is shown as a yellow ribbon. Side chains of Ile173 (red) and Tyr174 (green) are shown in stick figures, and the surface of residues Leu325 and Val328 is shown in blue.

exchange activity of Vav is contained in the DH domain (*10*, *11*).

Previous studies have shown that regulation of the DH domain GEF activity is important for normal cellular function and that loss of regulation through mutations and/or truncations of the Vav1 N-terminus can cause cellular transformation (*13*). Deletion of the first 66 residues leads to the originally discovered oncogenic version of Vav1 (*11*, *15*). Transfection of N-terminally truncated Vav1 into NIH 3T3 fibroblasts results in transformation, with the degree of transformation dependent upon the extent of the Ac region deletion (*13*, *14*). Deletion of the entire N-terminus, including the Ac region, results in phosphorylation independent Vav1 transformation activity (*16*). N-Terminal deletions also increase the GEF activity of Vav1, suggesting that unregulated GEF activity is the root cause of Vav1-mediated cellular transformation (*6*, *10*, *13*).

In normal cells, Vav1 is thought to be activated significantly by the phosphorylation of tyrosine residues in the Ac region (*15*, *17*−*20*). In particular, Tyr174 has been identified as a key regulatory site. Phosphorylation of this residue activates the GEF activity of various Vav proteins in vitro (*10*, *13*, *15*), and its mutation enhances the transforming activity of Vav1 in vivo (*13*, *15*, *17*, *20*). NMR studies of the minimal autoinhibited protein, which contains the DH domain and a portion of the Ac region, including Tyr174 revealed the physical basis of this core regulatory module (*6*). In the solution structure of this fragment, the sequence surrounding Tyr174 forms a helix that binds in the active site of the DH domain, blocking its access to substrates (Figure 1b) (*6*). Further NMR analyses showed that phosphorylation of Tyr174 displaces the helix from the DH domain, relieving autoinhibition (*6*). A recent single particle electron microscopy study of full length Vav3 showed that multiple domains of the molecule fold together to form a compact structure in the nonphosphorylated state (*21*). The DH−helix interactions of the minimal autoinhibited module appear to be retained in the full length protein, but are likely energetically modulated by interactions observed between the CH domain and the CRD. Phosphorylation causes large quaternary rearrangements that significantly decrease compactness (*21*), suggesting that the conformational changes in the minimal element can occur cooperatively with other domain rearrangements in the full length system. A complete understanding of this complex system will require first a quantitative understanding of the minimal autoinhibitory element, and then discovery of how the structure, thermodynamics, and kinetics of this module are affected by other domains in the protein.

In addition to Tyr174, the Vav1 Ac region contains two additional tyrosines, Tyr142 and Tyr160. All three sites contain the amino acid sequence ΦYxxΦ (where Φ = I, L, or V and X = any amino acid), which is a consensus substrate motif for Src family kinases (*22*, *23*). The conserved sequences containing Tyr142, Tyr160, and Tyr174 will be referred to hereafter as the Y1, Y2, and Y3 motifs, respectively, denoting the relative position of each from the N-terminus (Figure 1a). All three tyrosine motifs are phosphorylated as a part of Vav1 activation in vivo by Src and Syk family tyrosine kinases (*13*, *15*−*17*, *19*, *24*). Given their sequence similarity and proximity to the DH domain, it has been suggested that all three tyrosine residues may play a role in the activation and/or regulation of the Vav1 DH domain and that function(s) of these tyrosine motifs are important to our understanding of full length Vav1 (*13*, *16*, *19*).

Here we describe structural and biochemical studies of the three Ac region tyrosine motifs and their roles in regulating the DH domain. NMR data indicate that in the Ac-DH protein the Y1 and Y2 motifs do not interact appreciably with the DH domain and are likely free and disordered in solution both before and after phosphorylation. Consistent with this notion, the Lck mediated phosphorylation kinetics of the Y1 and Y2 motifs are nearly identical in the isolated peptides and in the context of the DH domain. In contrast, phosphorylation of the Y3 motif is reduced 15-fold in the context of the DH domain relative to the corresponding Y3 peptide. Combined thermodynamic and kinetic data demonstrate that phosphorylation at Y3 can be enhanced 4-fold through prior phosphorylation at Y1, which provides a docking site for the Lck SH2 domain. Taken together these observations support a model in which exposed tyrosine sites can be used as docking sites to gain access to the buried Y3 substrate, leading to rapid activation of Vav1 GEF activity.

MATERIALS AND METHODS

Molecular Constructs

Throughout the manuscript the sequence motifs surrounding Tyr142, Tyr160, and Tyr174 are referred to as Y1, Y2, and Y3, respectively (Figure 1a). Mutation of tyrosine in a motif to Phe or Asp is denoted by F or D, respectively. For

example, mutation of Tyr174 to Phe is denoted by F3. Phosphorylation of a tyrosine is indicated by pY, such that phosphorylated Tyr160 is indicated by pY2. A full list of Vav1 protein fragments used in this work is provided in Table S1 (Supporting Information).

Vav1 fragments Y1-Y2-Y3-DH (residues 138−375), Y2-Y3-DH (residues 155−375), and Y3-DH (residues 170−375) were generated by PCR from Vav1 cDNA (a gift from Dan Broek, University of Southern California) and subcloned into a modified pET15b vector (Novagen) containing an N-terminal Maltose Binding Protein (MBP) fusion tag and a TEV protease site. The acidic region tyrosine motif peptides used in kinase assays were generated by subcloning PCR fragments into a modified pET19b vector containing an N-terminal His_{10}-ubiquitin fusion protein with a TEV protease site to generate peptides containing residues 138−190 (all three tyrosine motifs) and 155−190 (only tyrosine motifs Y2 and Y3) (*25*). In the former peptide, Tyr160 and Tyr174 were mutated to Phe to give pep-Y1, which was used to measure intrinsic phosphorylation kinetics of Tyr142. In the latter peptide, Tyr174 was mutated to Phe to give pep-Y2, and Tyr160 was mutated to Phe to give pep-Y3, which were to measure intrinsic phosphorylation kinetics of Tyr160 and Tyr174, respectively. Baculoviruses expressing His_6-tagged Lck fragments SH2-Kin (residues 119−509), SH2*-Kin (residues 119−509, Arg154Lys mutation), and Kin (residues 225−509) were generated using the Fastbac system (Gibco) from Lck cDNA (a gift from Nicolai Van Oers, UT Southwestern Medical Center). Lck SH32 (residues 53−226 spanning both SH3 and SH2 domains) was expressed from a pET11a vector. Point mutations were generated using the Quick Change mutagenesis kit following the manufacturer's (Strategene) recommendations (see Table S1).

Protein Expression and Purification

Vav1 Proteins and Peptides. All Vav1 proteins and peptides were expressed in *Escherichia coli* strain BL21-(DE3) (Novagen), grown at 37 °C to $OD_{600} = 0.6$, and induced with 1.0 mM IPTG. Upon induction, cells were transferred to 20 °C and shaken for 10 h, or maintained at 37 °C for 4−6 h, for the Vav1 DH proteins and peptides, respectively. Vav1 proteins for NMR were expressed similarly in M9 minimal media, with $^{15}NH_4Cl$ and $^{13}C_6$-glucose as the sole nitrogen and carbon sources. All proteins and peptides were purified by anion-exchange chromatography (DEAE followed by MonoQ), followed by size exclusion chromatography (Superdex-75). In all cases, fusion tags were removed by Tev protease (Invitrogen) at 25 °C for 3−5 h in buffer containing 50 mM Tris-Cl, pH 7.5, 10 mM DTT, and 50−250 mM NaCl. Fusion tags were separated from Vav1 proteins/peptides by anion-exchange chromatography (MonoQ). All columns and column packing materials were obtained from Amersham Pharmacia/GE Healthcare. Following purification, all Vav1 proteins were either used in assays immediately or flash frozen in liquid nitrogen and stored at −80 °C for future use. The purity of all Vav samples was assessed by SDS−PAGE analyses, and representative gels are shown in Figure S3 (Supporting Information). All peptide and protein concentrations were measured using the following extinction coefficients at 280 nm: 13 640 M^{-1} (Y1-Y2-Y3-DH), 12 360 M^{-1} (Y1-D2-Y3-DH, Y2-Y3-DH), 11 080 M^{-1} (Y1-D2-D3-DH, D2-Y3-DH, Y2-D3-DH, and Y3-DH), and 1400 M^{-1} (Y1-F2-F3-pep, Y2-F2-pep, F2-Y3-pep).

Lck Kinase Proteins. All Lck kinase proteins were expressed from baculovirus in *Spodoptera frugiperda* (sf9) cells and harvested 60−72 h after infection. Cells were lysed with a Dounce homogenizer in 50 mM Tris-Cl, pH 7.5, 50 mM NaCl, 20 mM β-mercaptoethanol (His buffer A), and protease inhibitors. Lysate was clarified by centrifugation prior to Ni^{2+}−NTA affinity chromatography (Qiagen). Following a wash with His buffer A containing 20 mM imidazole, proteins were eluted from Ni^{2+} affinity columns with His buffer A containing 500 mM imidazole. The His_6-tag was removed by Tev digestion prior to further purification by ion exchange (MonoQ) and size exclusion chromatographies (Superdex-75). Aliquots of Lck kinase were flash frozen in liquid nitrogen and stored at −80 °C prior to use. Lck SH32 was expressed in *E. coli* strain BL21(DE3) and purified from cleared lysate by ion-exchange (DEAE and Source S15) and size exclusion chromatographies (Superdex-75) and used directly in assays or frozen at −80 °C prior to use. The purity of the final Lck SH32, Lck SH2*-Kin, and SH2-Kin samples was assessed by SDS−PAGE analyses (see Figure S3, lanes 11, 12, and 13, respectively). All kinase constructs were activated by incubating in 20 mM Tris-Cl, pH 7.5, 2 mM ATP, 10 mM $MgCl_2$, and 2 mM DTT for 30 min at 25 °C prior to use.

Phosphorylated Vav1 Proteins. All mono- and diphosphorylated Vav1 proteins were prepared by treating 200 μM Y2-Y3-DH or Y1-D2-Y3-DH with 200 nM Lck kinase domain in a reaction mixture containing 50 mM HEPES (pH 7.5), 50 mM NaCl, 10 mM DTT, 10 mM $MnCl_2$, 10 mM $MgCl_2$, and 5 mM ATP. Reactions were carried out at 30 °C for 30−40 min and quenched by addition of 10 mM EDTA, followed by passage through a HiTrap desalting column (Pharmacia) to remove unreacted ATP. The non-, mono-, and diphosphorylated proteins were separated by anion-exchange chromatography (see Figure 2; MonoQ, buffer A (20 mM Tris-Cl, pH 7.5, 50 mM NaCl, 5 mM DTT, 1 mM EDTA), buffer B (buffer A with 1 M NaCl)). The identity of each species was confirmed by mass spectrometry (indicating the number of phosphorylation sites) in combination with N-terminal amino acid sequencing (indicating the site of phosphorylation), and the purity was assessed by SDS−PAGE (See Figure S4, Supporting Information). Monophosphorylated proteins used in affinity measurements were prepared using D2-Y3-DH, Y2-D3-DH, and Y1-D2-Y3-DH substrates to produce pY2-D3-DH, D2-pY3-DH, and pY1-D2-Y3-DH, respectively.

Phosphotyrosine Peptides. Synthetic phosphopeptides corresponding to pTyr142 (DEDI^{142}pYSGLSDQID), pTyr160 (DEDL^{160}pYDCVEKEEAE), and pTyr174 (GDEI^{174}-pYEDLMRLESV) were obtained from the UT Southwestern Medical Center Protein/Peptide Core facility. All peptides were lyophilized twice from H_2O and dissolved in 50 mM HEPES, pH 7.5, 50 mM NaCl, 10 mM β-mercaptoethanol, and 1 mM EDTA. NaOH was used to adjust pH to 7.5, if necessary. All peptide concentrations were estimated using the previously reported extinction coefficient for pTyr (695 M^{-1} cm^{-1} at 268 nm, pH 7.5) (*26*).

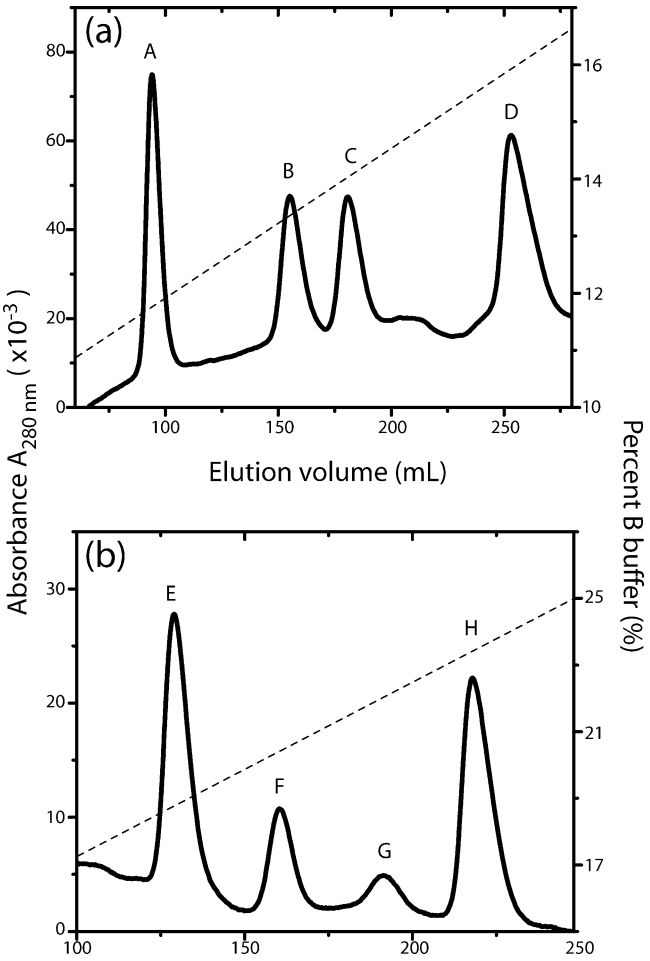

FIGURE 2: Anion-exchange chromatography allows the separation of singly and doubly phosphorylated Vav1 proteins. Chromatographic traces show the separation of nonphosphorylated, singly phosphorylated, and doubly phosphorylated species for (a) Y2-Y3-DH and (b) Y1-D2-Y3-DH proteins. In each chromatogram, elution volume is plotted against the absorbance at 280 nm (solid line left *Y* axis) and the percent buffer B (dashed line right *Y* axis). Peaks labeled A, B, C, and D represent Y2-Y3-DH, pY2-Y3-DH, Y2-pY3-DH, and pY2-pY3-DH. Peaks labeled E, F, G, and H represent Y1-D2-Y3-DH, pY1-D2-Y3-DH, Y1-D2-pY3-DH, and pY1-D2-pY3-DH, respectively. Details of the chromatographic separation are described in Materials and Methods, and the data from mass spectrometry analyses of these chromatographic peaks are summarized in Table 1.

NMR Experiments

All NMR experiments were carried out on Varian Innova NMR spectrometers operating at either 600 or 800 MHz ^{1}H frequency. Constant time ^{1}H/^{13}C HSQC spectra were recorded with 1536 (600 MHz) or 1706 (800 MHz) complex points and a sweep width of 9000 Hz (600 MHz) or 10 000 Hz (800 MHz) in the ^{1}H dimension, and 256 complex points and a sweep width of 9500 Hz (600 MHz) or 8000 Hz (800 MHz) in the ^{13}C dimension. All spectra were processed with nmrPipe software (*27*) and analyzed with either nmrDraw (*27*) or nmrview software (*28*).

Phosphorylation Kinetics

Spectrophotometric Coupled Assay. Phosphorylation kinetics of the peptides and protein substrates were measured using a spectrophotometric assay that couples the production of ADP to the oxidation of NADH stoichiometrically. Reactions were carried out in a Beckman DU800 spectrophotometer equipped with a Peltier temperature control unit. Samples were preincubated at 30 °C, and all reactions were carried out at 30 °C as described previously (*29*, *30*). Phosphorylation reactions were carried out in 50 mM HEPES, pH 7.5, 50 mM NaCl, 10 mM DTT, 2 mM ATP, 10 mM $MnCl_2$, 10 mM $MgCl_2$, 1 mM phosphoenolpyruvate, 0.2 mM NADH, 89 units/mL pyruvate kinase, 124 units/mL lactate dehydrogenase, by varying enzyme and/or substrate concentration. All phosphorylation kinetic parameters were derived from reactions containing either 100−200 nM SH2-Kin or 100−200 nM SH2*-Kin and substrate concentrations of up to 5 × K_M (peptides) and 0.2−1.0 × K_M (DH proteins). Thus, for the protein substrates, only k_{cat}/K_M could be directly determined. All kinase reactions were performed at least in duplicate and at least on two different occasions. Kinetic parameters are reported as an average and standard error.

Radioactive Kinase Assay. Due to limited availability, radioisotope (^{32}P) based kinase assays, with higher sensitivity, were used to study monophosphorylated protein substrates. These assays were carried out at 30 °C in 30 μL reactions containing 50 mM HEPES, pH 7.5, 50 mM NaCl, 10 mM DTT, 2 mM ATP (3000 μCi/mL specific activity), 10 mM $MnCl_2$, 10 mM $MgCl_2$, and 20 nM kinase. Substrate concentrations ranged from 16 to 66 μM. In the initial velocity assays, 6 μL aliquots were removed and the reaction was quenched by addition of 2× SDS loading buffer at 2, 4, and 8 min (<10% completion). Following SDS−PAGE, gels were dried and phosphate incorporation was measured by phosphoimaging. A single site substrate, D1-D2-Y3-DH, was used to confirm that the activities of SH2-Kin and SH2*-Kin were identical. The relative effects of the kinase SH2 domain was further assessed by measuring phosphorylation of either D1-D2-Y3-DH or pY1-D2-Y3-DH substrate (25 μM) and Lck SH2-Kin or SH2*-Kin (20 nM) in the presence or absence of Lck SH32 domains (150 μM). For analysis, 5 μL aliquots were (three aliquots each) quenched with 5 μL of 2× SDS buffer at 8 min after initiating the reaction by kinase addition. Since the concentration and the time chosen were in the linear regime, the relative differences in phosphate incorporation are directly proportional to their effective k_{cat}/K_M values.

Isothermal Titration Calorimetry (ITC)

Affinity measurements between the Lck SH2 domain and phosphoproteins/peptides were carried out at 25 °C using a VP-ITC microcalorimeter (Microcal Corp, Northampton, MA). Prior to use, Lck SH32 and monophosphorylated Vav1 DH proteins (pY1-D2-Y3-DH, pY2-D3-DH, and D2-pY3-DH) were dialyzed against 1 L of 50 mM HEPES, pH 7.5, 50 mM NaCl, 10 mM BME, and 1 mM EDTA over 24 h with two buffer changes. Tyrosine motif peptides were dissolved in the same dialysis buffer. Exothermic heats of reaction (μcal/s) were measured for up to 30 injections of the phosphotyrosine ligand (150−220 μM) into the Lck SH32 protein (20−22 μM). All data were baseline corrected by subtracting heats from the ligand injection into a buffer only sample. Raw calorimetry data were processed and nonlinear least squares fit to yield n (number of binding sites), K_D (equilibrium binding constant), and ΔH (change in enthalpy of reaction), using the ORIGIN software package.

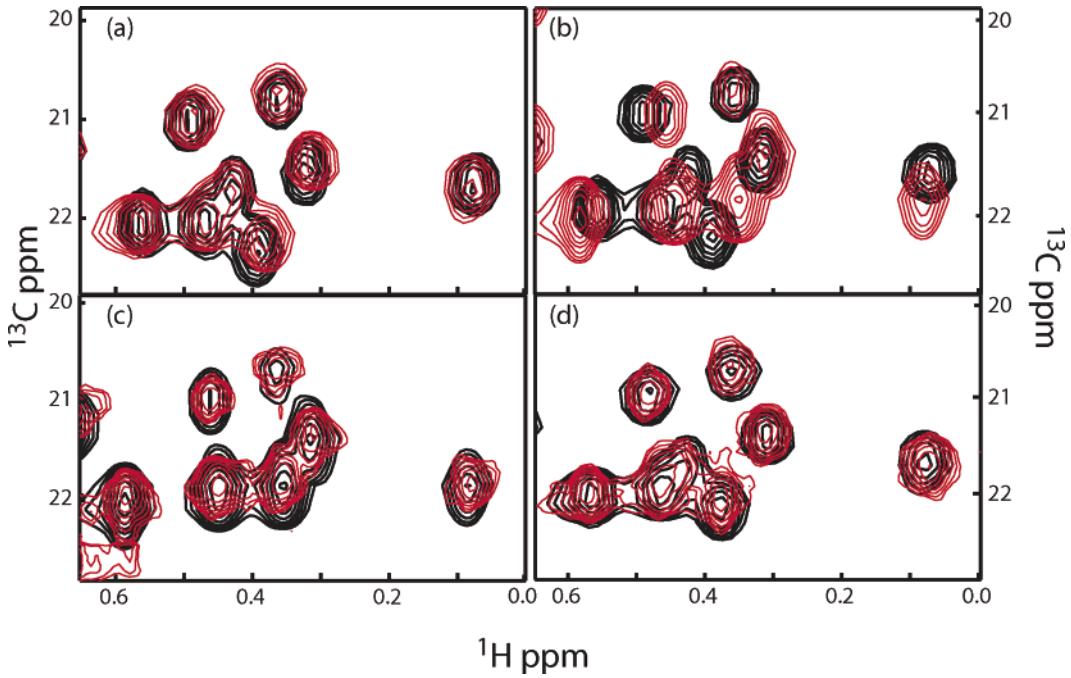

FIGURE 3: Phosphorylation at Tyr174 in the Y3 motif induces similar changes in Y3-DH and Y1-D2-Y3-DH. Methyl regions of constant time ^{1}H/^{13}C HSQC spectra of (a) Y3-DH (black) and Y1-D2-Y3-DH (red), (b) Y3-DH (black) and pY3-DH (red), (c) pY3-DH (black) and Y1-D2-pY3-DH (red), and (d) Y1-D2-Y3-DH (black) and pY1-D2-Y3-DH (red).

Reported binding values are an average of at least 2 experiments.

Kinetic Simulations

The kinetic simulation software package GEPASI version 3.30 (http://www.gepasi.org) was used to model the phosphorylation profiles of three site substrates either with (Y1-Y2-Y3-DH) or without (residues 138−190) the DH domain (*31*). Experimentally determined K_M (Henri−Michaelis−Menten constant) and k_{cat} (catalytic rate constant) values for the single site substrates (Tables 2, 3, and 5) were used in the simulations. All reactions and kinetic parameters are shown in schematic form in Figure S1 and Table S2 (Supporting Information). We assumed in the simulations that the phosphorylation kinetics at Y1 and Y2 are not affected by initial phosphorylation at Y2/Y3 and Y1/Y3, respectively. In practice, docking of SH2-Kin to initially modified sites could affect phosphorylation kinetics at Y1 or Y2. However, additional simulations (not shown) demonstrated that even a 10-fold increase in k_{cat}/K_M for Y1 or Y2 due to prior phosphorylation elsewhere had virtually no effect on the Y3 phosphorylation profile. Since Y3 phosphorylation is the only event that directly regulates DH activity, and is the focus of our investigation here, our assumptions are valid in this context. GEPASI files used in the simulations are available from the authors. Each simulation was carried out for a time period of 15 min, and 300 points were obtained for further analyses. An initial substrate concentration of 100 μM was used in all cases. The kinase, either SH2*-Kin or SH2-Kin, was set to 1 μM. Normalized total pY1 was calculated by dividing the total pY1 species (pY1-Y2-Y3 + pY1-pY2-Y3 + pY1-Y2-pY3 + pY1-pY2-pY3) by the initial substrate concentration; normalized pY3 was calculated analogously.

RESULTS

Only the Y3 Tyrosine Motif Interacts with the DH Domain. In the constant time ^{1}H/^{13}C HSQC spectra, methyl resonances representing the Y3 inhibitory arm and the DH domain are nearly identical in both the Y3-DH and Y1-Y2-Y3-DH constructs (Figure 3a, Figure S2, Supporting Information). Comparison of the corresponding ^{1}H/^{15}N HSQC spectra of Y3-DH and Y1-Y2-Y3-DH revealed similar correlations with the exception of a number of new resonances corresponding to the Y1-Y2 region of the larger construct (not shown). These new resonances displayed poor chemical shift dispersion and were more intense, suggesting disorder in the Y1-Y2 region. Consistent with this observation, the methyl region of the ^{1}H/^{13}C HSQC spectrum of Y1-Y2-Y3-DH contains 12 new resonances, which are intense and narrow (Figure S2). These data indicate that the contacts between the Y3 motif and the DH catalytic domain observed in the Y3-DH structure (*6*) are maintained in the context of the Y1-Y2-Y3-DH construct, and that the Y1 and Y2 motifs in the latter are likely disordered in solution.

In the structure of Y3-DH (Figure 1b), the Y3 motif interacts with a number of hydrophobic residues in the DH domain active site, including Phe320, Leu325, and Val328 (*6*). In all three Vav1 tyrosine motifs, two methyl bearing residues are located at $i - 1$ and $i + 3$ from the tyrosine residue (Figure 1a). Therefore, we used the methyl region of ^{1}H/^{13}C HSQC spectra to characterize structural changes in the Vav1 Ac and DH domains upon phosphorylation. Previous data revealed a number of resonance shifts in both ^{1}H/^{15}N and ^{1}H/^{13}C HSQC spectra upon phosphorylation due to structural changes in both the inhibitory Y3 motif and residues within the DH domain (*6*). These include large chemical shift changes in the methyl region of the ^{1}H/^{13}C HSQC spectrum of Y3-DH (Figure 3b) and the collapse of amide resonances for the Y3 motif to random coil values in

Table 1: Mass Spectrometry Analysis of Phospho Vav1 Constructs Separated by Ion-Exchange Chromatography

construct	calcd mass (Da)	exptl mass (Da)	peak in Figure 2
Y2-Y3-DH	26 302	26 304 ± 1	A
pY2-Y3-DH	26 382	26 384 ± 2	B
Y2-pY3-DH	26 382	26 384 ± 2	C
pY2-pY3-DH	26 462	26 464 ± 2	D
Y1-D2-Y3-DH	28 251	28 252 ± 1	E
pY1-D2-Y3-DH	28 331	28 332 ± 1	F
Y1-D2-pY3-DH	28 331	28 332 ± 1	G
pY1-D2-pY3-DH	28 411	28 412 ± 1	H

Table 2: Kinetic Parameters of Phosphorylation of the Vav1 Tyrosine Motif Peptides

substrate	k_{cat}/K_M ($\times 10^5$ M^{-1} min^{-1})	K_M (μM)	k_{cat} (min^{-1})
pep-Y1	7.34 ± 0.01	166 ± 5	122 ± 3
pep-Y2	2.83 ± 0.02	378 ± 22	107 ± 14
pep-Y3	21.4 ± 0.01	68 ± 2	144 ± 4

the $^1H/^{15}N$ HSQC spectrum (not shown). Nearly identical chemical shift changes in the Y3 motif and the DH domain are observed for the Y3-DH or Y1-D2-Y3-DH constructs when selectively phosphorylated at Tyr174 (Figure 3c). In contrast, no significant chemical shift changes are observed in the Y3 motif or the DH domain when the Y1 motif is specifically phosphorylated in the Y1-D2-Y3-DH construct (Figure 3d). Similarly, no significant changes are observed in Y3 or DH when Y2 is phosphorylated in Y1-Y2-DH (not shown). These observations further confirm that in Ac-DH constructs the Y1 and Y2 motifs are free in solution, and demonstrate that phosphorylation of these motifs does not significantly affect interactions of the DH domain with the Y3 motif.

The Y3 Tyrosine Motif Is Protected from Phosphorylation by the DH Domain. The Src family tyrosine kinase Lck phosphorylates Vav1 downstream of activated cell surface receptors such as the T cell, B cell, and Fcγ receptors (*32*, *33*). Therefore, we used a recombinant Lck kinase domain to evaluate the phosphorylation kinetics of the Vav1 acidic region tyrosine motifs. To learn how intramolecular interactions in Vav1 affect phosphorylation kinetics, we compared Lck activity toward the tyrosine motifs in free peptides and in the DH domain constructs. Peptides containing the individual Y1, Y2, and Y3 tyrosine motifs were used to measure initial reaction rates using a range of peptide concentrations (0.0−2.2 mM, Figure S5, Supporting Information) in a coupled assay (squares in Figures 4a, b, and c, respectively, summarized in Table 2) (*29*, *30*). By fitting the initial rate data to the Michaelis−Menten equation, we obtained k_{cat}/K_M values of 7.34 ± 0.01 × 10^5 M^{-1} min^{-1}, 2.83 ± 0.02 × 10^5 M^{-1} min^{-1}, and 21.4 ± 0.01 × 10^5 M^{-1} min^{-1} for pep-Y1, pep-Y2, and pep-Y3, respectively. While the k_{cat}/K_Mvalues for pep-Y1 and pep-Y2 are similar, the k_{cat}/K_M for pep-Y3 is approximately 3−6-fold higher, indicating that the Y3 motif is intrinsically a better Lck substrate than Y1 or Y2. The k_{cat}/K_m values obtained for Vav1 peptides here are similar to those obtained for other Src family kinases with peptide substrates. For example, Pellicena et al. reported that tyrosine phosphorylation of a peptide substrate by Hck occurred with a k_{cat}/K_M of 3.0 × 10^5 M^{-1} min^{-1} (*30*).

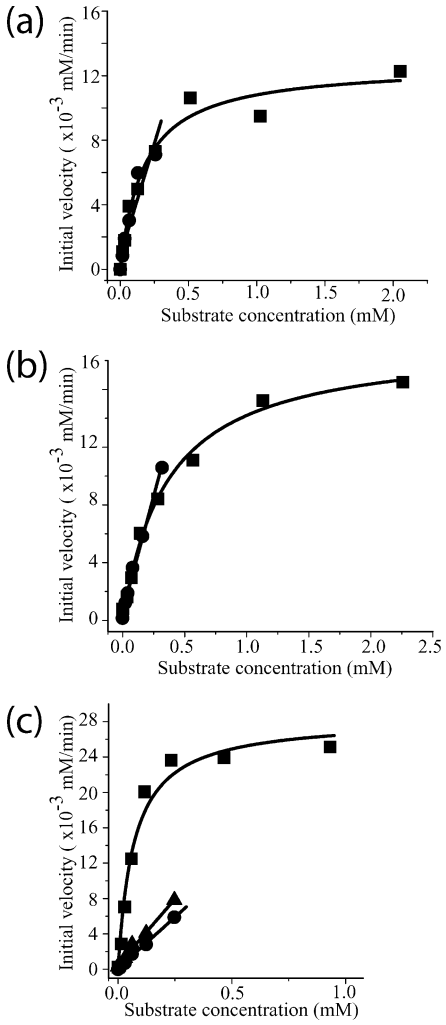

FIGURE 4: Phosphorylation kinetics of tyrosine motifs in the Vav1 Ac region by the Lck kinase domain. (a) Phosphorylation of pep-Y1 (squares) and Y1-D2-D3-DH protein (circles). (b) Phosphorylation of pep-Y2 (squares) and Y2-F3-DH protein (circles). (c) Phosphorylation of pep-Y3 (squares), D2-Y3-DH (triangles), and D1-D2-Y3-DH (circles). Reactions were carried out with 100 nM (a and b) or 200 nM (c) kinase. Kinetic parameters are summarized in Tables 2 and 3. Lines show fits of the initial rate data to the Michaelis−Menten equation (for pep-Y1, pep-Y2, and pep-Y3) or to a straight line (for all other substrates).

Table 3: Kinetic Parameters for Phosphorylation of the Vav1 Tyrosine Motif in the Context of the DH Domain

substrate	k_{cat}/K_M ($\times 10^5$ M^{-1} min^{-1})	$(k_{cat}/K_M)_{peptide}/(k_{cat}/K_M)_{DH}$
Y1-D2-D3-DH	5.38 ± 0.42	~1
Y2-D2-DH	2.04 ± 0.17	~1
D2-Y3-DH	1.39 ± 0.23	~15

Next, we evaluated the ability of the Lck kinase domain to phosphorylate tyrosine motifs that are tethered to the DH domain. These assays were conducted at relatively low substrate concentrations to avoid complications from protein aggregation. Under these conditions we were unable to measure k_{cat} and K_M individually, but we were able to extract their ratio from the initial velocity vs substrate curves. We obtained k_{cat}/K_M values of 5.38 ± 0.42 × 10^5 M^{-1} min^{-1} and 2.04 ± 0.01 × 10^5 M^{-1} min^{-1} for the Y1-D2-D3-DH and Y2-D3-DH constructs, respectively (Figure 4 and Table 3). These values are very similar to those of the isolated

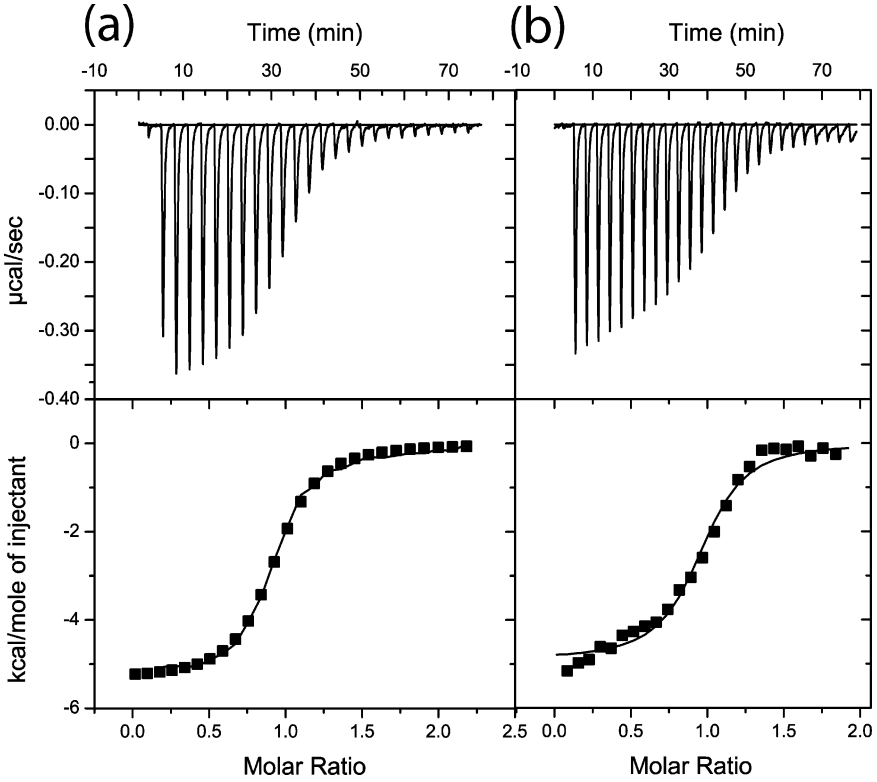

FIGURE 5: Lck SH2 domain binds Vav1 phosphotyrosine motifs with high affinity. Representative ITC data for Lck SH32 binding to (a) peptide DEDL[160]pYDCVEKEEAE, representing pY2 and (b) pY2-D3-DH protein. Raw heats of reaction vs time (top panels) and the integrated heats of reaction vs molar ratio of ligand to receptor (bottom panels) are plotted. All experiments were repeated at least twice, and the data obtained are summarized in Table 4.

Table 4: Thermodynamic Binding Parameters for Lck SH2 Domain Interaction with Vav1 Phosphotyrosine Motifs

ligand	*n* (no. of sites)	K_D (μM)	$\Delta G°$ (kcal/mol)	$\Delta H°$ (kcal/mol)	$-T\Delta S°$ (kcal/mol)
pY1 peptide	1.02 ± 0.04	0.80 ± 0.03	−8.32 ± 0.03	−4.64 ± 0.18	−3.68 ± 0.15
pY2 peptide	0.97 ± 0.01	0.37 ± 0.01	−8.71 ± 0.06	−4.82 ± 0.01	−3.89 ± 0.06
pY3 peptide	1.07 ± 0.01	0.89 ± 0.08	−8.25 ± 0.05	−3.92 ± 0.24	−4.32 ± 0.30
pY1-D2-Y3-DH	0.78 ± 0.10	1.39 ± 0.44	−7.77 ± 0.28	−4.59 ± 0.26	−3.18 ± 0.77
pY2-D3-DH	1.02 ± 0.10	0.52 ± 0.11	−8.57 ± 0.14	−4.46 ± 0.64	−4.11 ± 0.51
D2-pY3-DH	1.09 ± 0.06	0.36 ± 0.04	−8.77 ± 0.06	−5.30 ± 0.17	−3.47 ± 0.23

peptide substrates, indicating that the presence of the DH domain does not affect the catalytic efficiency of Lck toward the Y1 and Y2 motifs. In contrast, phosphorylation of D1-D2-Y3-DH and D2-Y3-DH (or F2-Y3-DH) occurred with approximately 15-fold lower k_{cat}/K_M compared to pep-Y3 (Figure 4c and Table 3). Although we were unable to measure k_{cat} and K_M directly, it is likely that the observed difference derives largely from an increase in K_M due to competition between the DH domain and the kinase for the Y3 site. This is a reasonable assumption given that the identity of the substrate (i.e. the sequence in the Y3 motif) remains the same in both the peptide and the Y3-DH construct. Thus, the DH domain significantly protects Y3 from phosphorylation but has little effect on Y1 and Y2, consistent with the structural data above.

The Lck SH2 Domain Binds Vav1 Phosphotyrosine Motifs with High Affinity. The tyrosine motifs within the Vav1 Ac domain (Y1-[142]YSGL, Y2-[160]YDCV, and Y3-[174]YEDL) are also reasonable consensus binding sequences for Src family SH2 domains (pY-D/E-x-Φ, where Φ = I, L, or V, and x is any other amino acid but mainly D or E (*34*). Therefore, we measured the affinity of each phosphotyrosine motif, both as a short synthetic peptide and as a singly phosphorylated DH domain, for the Lck SH2 domain by isothermal titration calorimetry (Figure 5, Table 4). All isotherms fit to a 1:1 binding model with K_D of 0.80 ± 0.03 μM, 0.37 ± 0.01 μM, and 0.89 ± 0.08 μM for the pY1, pY2, and pY3 peptides, respectively. Dissociation constants for the pY1-D2-Y3-DH, pY2-D3-DH, and D2-pY3-DH proteins are 1.39 ± 0.44 μM, 0.52 ± 0.11 μM, and 0.36 ± 0.04 μM, respectively. These values are similar to those reported for other phosphotyrosine-containing peptides binding to the Lck SH2 domain (*35*). Moreover, comparison of the calorimetry data for the phosphopeptides and phosphorylated DH constructs suggests that the SH2−phosphotyrosine interactions are unaffected by the DH domain. Therefore, the Lck SH2 domain can bind phosphorylated DH domain containing constructs with affinities similar to those of the isolated phosphopeptides.

Initial Binding Can Enhance Phosphorylation Rate at a Subsequent Site. Previous studies have shown that in substrates containing multiple tyrosines, initial phosphorylation at one site can enhance phosphorylation at nearby sites by SH2 containing Src family kinases through SH2−phosphotyrosine interactions (*30*). To determine whether phosphorylation at either Y1 or Y2 could affect phospho-

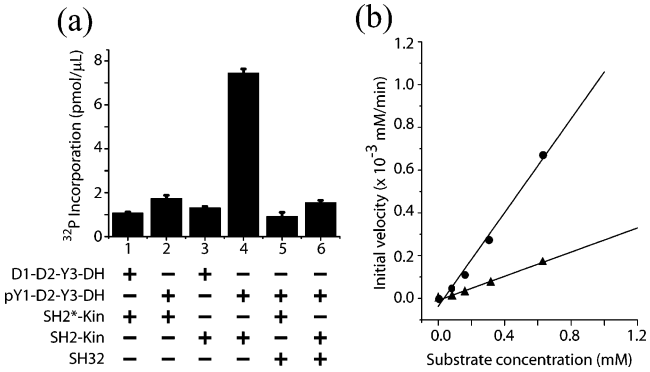

FIGURE 6: Docking of Lck SH2-Kin to pY1 enhances phosphorylation at Y3. (a) Phosphorylation of either D1-D2-Y3-DH or pY1-D2-Y3-DH (25 μM each) by Lck SH2*-Kin or Lck SH2-Kin (20 nM in both cases; lanes 1−4) and with saturating Lck SH32 (150 μM) (lanes 5 and 6). Reactions were carried out for 8 min, and the incorporated phosphate was measured by autoradiography as described in Materials and Methods. Components of all reactions are listed below the graph. (b) Initial rates of phosphorylation of pY1-D2-Y3-DH substrate by SH2-Kin (circles) or SH2*-Kin (triangles) vs substrate concentration.

rylation kinetics at Y3, we first generated the singly phosphorylated species pY2-Y3-DH and pY1-D2-Y3-DH on a preparative scale. Details of this procedure are provided in Materials and Methods. Substoichiometric phosphorylation of Y2-Y3-DH and Y1-D2-Y3-DH provided mixtures of starting material, mono- and diphosphorylated species. In both cases, all four possible species could be cleanly separated by anion exchange chromatography using a very shallow salt gradient (>6 column volumes per %B increase), as shown in Figures 2a and b. The number of phosphorylation sites in each peak was determined by mass spectrometry (Table 1). As expected on the basis of simple charge considerations, unphosphorylated starting material eluted first from the column (Figures 2a and b, peaks A and E), followed by the two monophosphorylated species (Figures 2a and b, peaks B/C and F/G), with the diphosphorylated protein eluting last (Figures 2a and b, peaks D and H). The exact identities of the singly phosphorylated materials were then determined by N-terminal amino acid sequencing. By optimizing reaction times and conditions, we were able to routinely produce 100−500 μg quantities of the desired singly phosphorylated species for use in Y3 phosphorylation assays below.

With the singly phosphorylated material in hand, we first compared the reaction kinetics of pY1-D2-Y3-DH to that of D1-D2-Y3-DH (and F1-F2-Y3-DH) using an Lck SH2-kinase construct that is defective in phosphotyrosine binding (SH2*-Kin, with Arg154Lys mutation). The two substrates were phosphorylated with similar kinetics, suggesting that pY1 does not significantly affect the phosphorylation kinetics when the Lck SH2 domain is mutated (reactions 1 and 2, Figure 6a). Similar results were obtained in a comparison of pY2-Y3-DH and D2-Y3-DH (or F2-Y3-DH) (data not shown). Thus, in the absence of a functional Lck SH2 domain, initial phosphorylation at Y1 or Y2 resulted in little difference in the rate of phosphorylation at Y3. In contrast, when the Lck SH2-Kin enzyme was used to phosphorylate pY1-D2-Y3-DH and D1-D2-Y3-DH, the pY1-D2-Y3-DH sample was phosphorylated appreciably more readily (reactions 3 and 4, Figure 6a). We further quantified this

Table 5: Kinetic Parameters of pY1-D2-Y3-DH Phosphorylation

enzyme	k_{cat}/K_M ($\times 10^5$ M^{-1} min^{-1})	$(k_{cat}/K_M)_{peptide}/(k_{cat}/K_M)_{DH}$
Lck SH2-Kin	4.8 ± 0.4	∼4
Lck SH2*-Kin	1.4 ± 0.4	∼16

observation by varying the pY1-D2-Y3-DH concentration (between 16 and 66 μM), which revealed a 4-fold increase in k_{cat}/K_M for SH2-Kin over SH2*-Kin (Figure 6b, Table 5). This effect does not appear to be due to an SH2-mediated change in the intrinsic kinase accessibility of Y3, since SH2 domain alone (at >10 times K_D of SH2 binding to pY1) did not enhance phosphorylation of pY1-D2-Y3-DH by SH2*-Kin (reactions 2 and 5, Figure 6a). Rather, the effect requires binding of SH2-Kin to pY1, since excess SH2 completely blocked enhancement of SH2-Kin relative to SH2*-Kin (reactions 2, 4, and 6, Figure 6a). Our NMR data support this supposition since, as described above, phosphorylation of Y1-D2-Y3-DH at Y1 does not significantly affect the resonances of the Y3-DH moiety in this protein (Figure 3). The combined NMR, SH2-binding, and kinetic data suggest that docking of the Lck SH2 domain to pY1 is the cause of the enhanced phosphorylation at Y3 by prior phosphorylation of Y1-D2-Y3-DH at Y1. This effect is likely due to a decrease in the substrate K_M, although we are unable to demonstrate this directly due to limitations in substrate solubility. Interestingly, the effect is specific to phosphorylation at Y1, since analogous experiments with pY2-Y3-DH showed that initial phosphorylation at Y2 has no effect on the kinetics of Y3 modification by SH2-Kin (not shown).

Kinetic Simulations of the Three Site Y1-Y2-Y3-DH Substrate Suggest Enhanced Phosphorylation of Y3 (and Activation) Due to SH2 Interactions with pY1. We have not yet developed experimental procedures to monitor the production of Y3 phosphorylated species (i.e. DH domain active species) during reaction of substrates containing all three tyrosine motifs, such as Y1-Y2-Y3-DH. However, since we have measured the kinetic parameters for reactions mimicking many of the individual phosphorylation events in this process, and can estimate the remainder, we can use simulations to understand how much the SH2 docking effects described in the previous section affect the activation kinetics of Y1-Y2-Y3-DH. The main results of these simulations are shown in Figure 7. In the presence of the Lck SH2*-Kin, total pY3 species are produced appreciably more rapidly in the reaction of a three-motif peptide (solid red curve) than of Y1-Y2-Y3-DH (dotted red curve), reflecting suppression of Tyr174 phosphorylation by the DH domain. Phospho-Y1 species are generated from Y1-Y2-Y3-DH at an intermediate rate due to the intrinsic preference of the kinase domain for Y3 (dotted blue curve, Table 2). Use of SH2-Kin results in significant changes in the production profile of the pY3 species. At early time points, pY3 generation is similar for SH2-Kin and SH2*-Kin (dashed and dotted curves, respectively, Figure 7a inset). However, as pY1 is produced, pY3 generation in the SH2-Kin reaction moves significantly ahead of that in the reaction with SH2*-Kin, reflecting the increase in k_{cat}/K_M due to docking of the former enzyme to its substrate. The maximum difference in pY3 production by the two kinase constructs is approximately 1.8-fold, as shown in Figure 7b. This increase in the Y3 phosphorylation rate as the reaction proceeds gives the production profile a

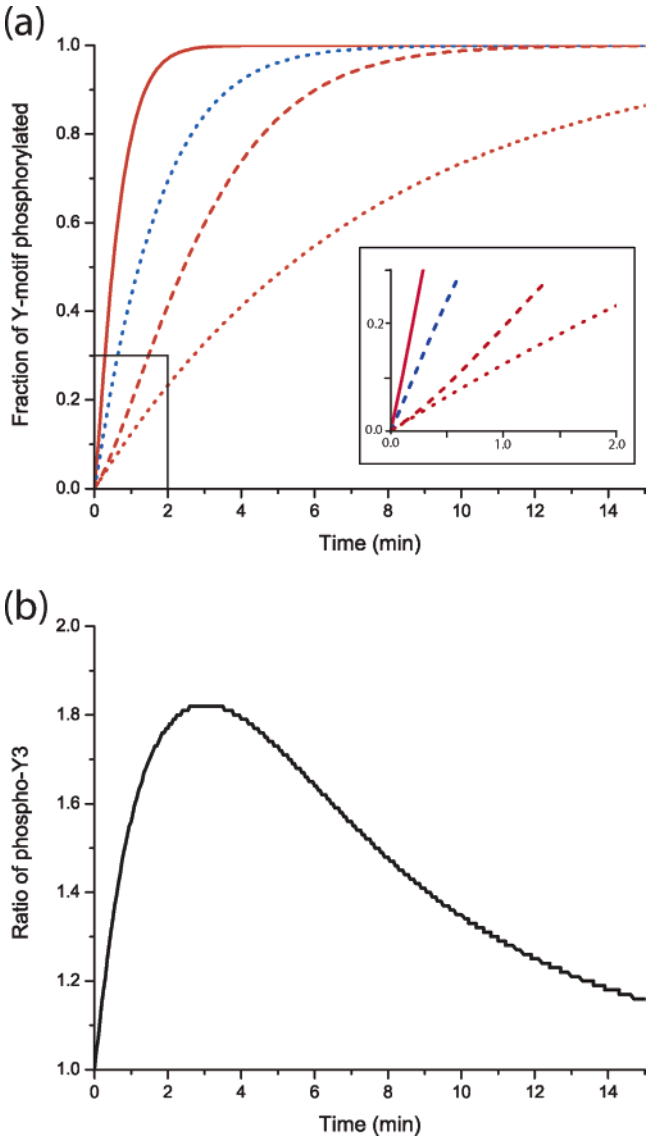

FIGURE 7: Kinetic simulations of Lck-mediated phosphorylation of Y1-Y2-Y3 proteins. (a) Red curves show production of total pY3 species as a fraction of initial substrate. Solid red curve shows reaction of a three-motif peptide (Y1-Y2-Y3, e.g. residues 138−190) with SH2*-Kin. Dashed red curve shows reaction of Y1-Y2-Y3-DH with SH2-Kin. Dotted red curve shows reaction of Y1-Y2-Y3-DH with SH2*-Kin. Dotted blue curve shows production of pY1 species in Y1-Y2-Y3-DH by SH2-Kin or SH2*-Kin (which have essentially identical kinase parameters toward Y1; note the simulations assume prior phosphorylation at Y2 or Y3 has no effect on phosphorylation at Y1, see Materials and Methods). Inset shows initial portion of curves. (b) Ratio of total pY3 species in reactions with SH-Kin and SH2*-Kin as a function of time for the Y1-Y2-Y3-DH substrate.

shallow sigmoidal shape, as shown in the Figure 7a inset. Thus, our experimental data and simulations indicate that while interactions between Y3 and the DH domain can substantially repress the rate of DH domain activation, this repression can be significantly alleviated by the ability of pY1 to serve as a docking site for Lck.

DISCUSSION

In this study, we have used a variety of Vav1 Ac peptide and Ac-DH protein constructs to study the role of the Ac region tyrosine motifs in autoinhibition of the DH domain and activation by tyrosine kinases. Our biochemical data indicate that the Y1 and Y2 motifs are not protected from phosphorylation relative to their corresponding peptide substrates, suggesting that these motifs in the Y1-Y2-Y3-DH construct do not interact with the DH domain and are likely free in solution. Our NMR data, based on a variety of mutations, truncations, and specifically phosphorylated samples, are also consistent with this conclusion. The absence of significant contacts between Y1 or Y2 and the DH domain, even in constructs where Y3 has been displaced by mutation, indicates that our previous hypothesis that these motifs may contribute to autoinhibition by binding the DH domain analogously to Y3 (*6*) is incorrect. It remains unclear how mutation or truncation of Y1 and Y2 leads to Vav1 activation (*11*−*13*). As has been suggested previously (*11*, *19*, *20*), pY1 and/or pY2 may recruit inhibitors of the GEF activity of the DH domain or of the activation of the DH domain. Alternatively, Y1 and Y2 may contribute to suppression of DH activity through cooperative effects involving interactions with other regions of the protein. Preliminary NMR data suggesting interactions of Y1 and Y2 with the CH domain in a CH-Ac-DH protein provide some support for the latter model (Amarasinghe and Rosen, unpublished), although much more data will be required to resolve this issue.

In contrast to Y1 and Y2, the Y3 motif is protected from phosphorylation 15-fold relative to the isolated peptide through previously described intramolecular interactions with the DH domain (*6*). In the autoinhibited structure, the Tyr174 side chain is buried in the interface between the Y3 helix and the DH domain, preventing the kinase from accessing Tyr174 in the ground state of the system. Tyrosine kinases in general bind and phosphorylate substrates that are in extended conformation (*5*, *36*). For example, in the crystal structure of the insulin receptor kinase (IRK) bound to a peptide substrate, the peptide substrate forms an extended antiparallel β-strand along the activation loop (*36*). Given the similarities between the Lck and IRK kinase domains, especially in the activation loop and active site, Lck likely binds its substrate peptides in a similar manner (*36*, *37*). The helical conformation observed for the Y3 motif in the autoinhibited DH domain structure is thus inconsistent with the structural requirements for kinase recognition. Therefore, the ability of Lck to phosphorylate Tyr174 suggests the existence of an excited state (or states) where the tyrosine side chain is exposed and the Y3 helix is at least partially destabilized, providing access to kinase. An equilibrium between a ground state, with the helix bound to the DH domain, and at least one other excited state, where the helix is dissociated from the DH domain, can account for our observed data. Namely, the proposed model shown in Figure 8 could both account for the ability of Lck to phosphorylate Y3 in the context of the DH domain and also explain the lower phosphorylation rates observed for the Y3 site in the presence of the DH domain (Figure 8a). An excited state conformation, as proposed in this model, could be either weakly populated in the free protein or induced by initial interactions with the kinase. Our current data do not allow us to distinguish between these two kinetic pathways. Since the phosphorylation rate of autoinhibited Vav1 scales linearly with kinase concentration, the proposed equilibrium (more directly, the rate of the helix closing since the equilibrium is defined by the ratio of the helix opening and closing rates) must be fast relative to the rate of phosphorylation (see Figure

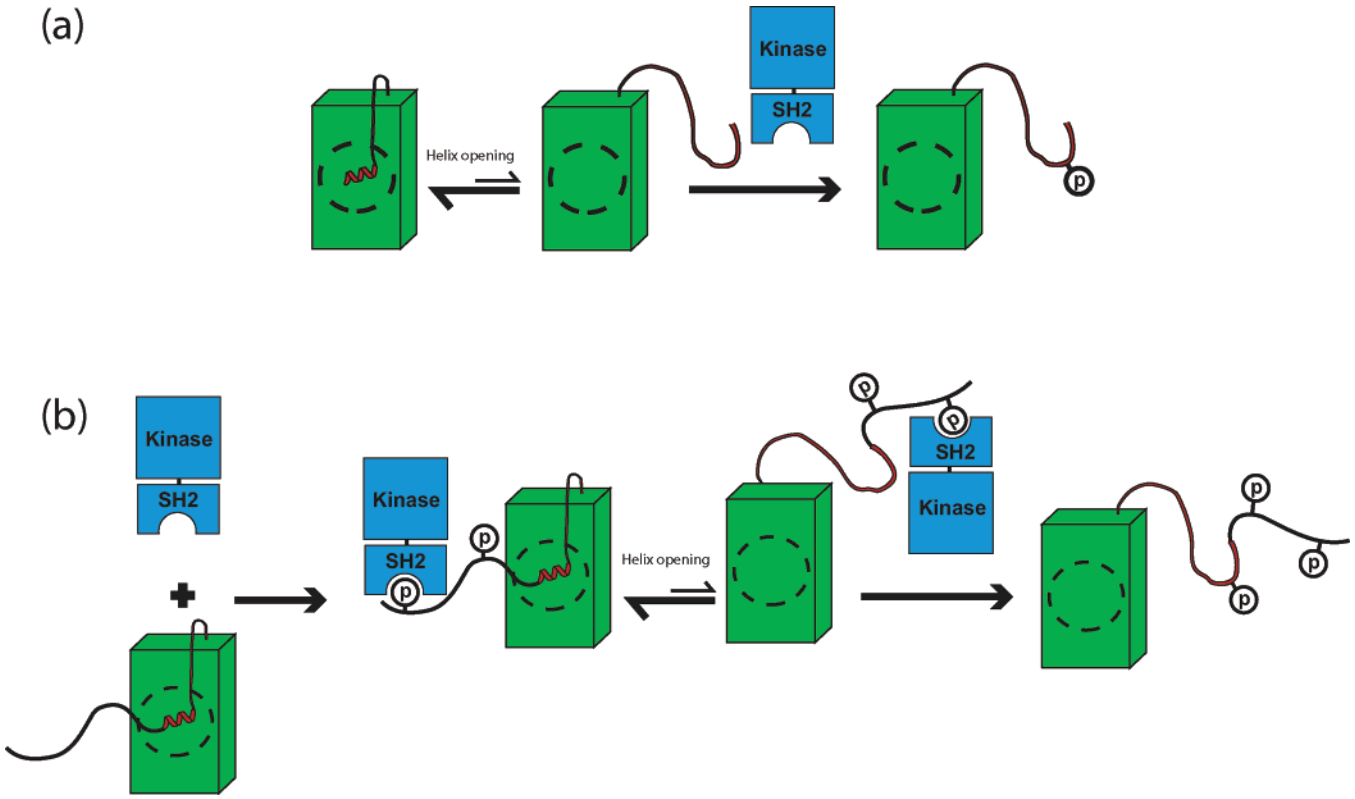

FIGURE 8: Access point model for relief of autoinhibition in the Vav1 DH domain. (a) The Y3-DH construct exists in an equilibrium between a closed state, where Tyr174 is protected from kinase, and an open state where Tyr174 is exposed. The equilibrium is strongly biased toward the closed state and overall phosphorylation kinetics are slow relative to a free Y3-containing peptide. (b) In the Y1-Y2-Y3-DH construct, Lck can initially phosphorylate the solvent exposed Y1 (and Y2) tyrosine motif(s), which can consequently act as a docking site for the Lck SH2 domain. The open−closed equilibrium is not affected by Y1 or Y2 phosphorylation or SH2 domain binding. Lck SH2 domain binding to pY1 allows the kinase to phosphorylate Y3 as an intramolecular substrate accelerating the overall phosphorylation kinetics. Thus, access point capture of an exposed docking site may provide a kinetic advantage in Vav1 activation by Lck.

8 and legend (*38*)). In such a scenario, the observed phosphorylation rates are governed by the relative populations of the ground and excited states. In the simplest case of a two-state equilibrium, the 15-fold difference we observe in k_{cat}/K_M for Y3 phosphorylation between the Y3-containing peptide and Y3-DH (in either D1-D2-Y3-DH or D2-Y3-DH) would indicate that ~7% (1/15) of the autoinhibited protein exists in the excited state. The exact nature of this equilibrium and its role in Vav1 activation is a subject of further investigation in our lab (Li et al., in preparation).

When phosphorylated, the Y1, Y2, and Y3 motifs can each bind the Lck SH2 domain with similar μM affinities in both peptide and DH-containing systems. Consistent with this finding, initial phosphorylation of the Y1 motif leads to a 4-fold increase in k_{cat}/K_M at the critical Y3 position by SH2-containing kinase constructs. Since the enhancement is specific to kinases with functional SH2 domains, it appears that the SH2 domain binds to the pY1 motif and enables the kinase domain to phosphorylate Y3 in intramolecular fashion. The addition of excess free SH2 domain to reactions containing SH2-Kin reduced the rate to that of SH2*-Kin. Thus, the observed rate enhancement for SH2-Kin is due to direct association of the kinase to pY1 rather than conformational changes induced by binding of the SH2 domain to the pY1 site. Our kinetic simulations indicate that when Y1-Y2-Y3-DH is phosphorylated, the ability of SH2-Kin to dock on pY1 can substantially enhance phosphorylation at the critical Y3 site (compare dashed and dotted red curves in Figure 7).

The role of Src family kinase SH2 domains in phosphorylation of multi-tyrosine substrates has been investigated previously in several systems. An elegant study by Miller and co-workers found that initial phosphorylation of a peptide substrate for the Hck kinase led to a 10-fold increase in k_{cat}/K_M for phosphorylation at a subsequent site (*30*). This enhancement required a functional SH2 domain on the Hck kinase construct, and resulted from a decrease in K_M without a change in k_{cat}. These authors also observed the greatest increase in k_{cat}/K_M when the spacer between the initial phosphorylation site and the subsequent site was 12 residues. Although that study did not examine spacers longer than 12, the enhancement in k_{cat}/K_M was only 5-fold when a 7-residue spacer was used and was completely abolished when the spacer was reduced to 3 residues. However, they did not observe an orientational dependence between the initial and subsequent phosphorylation sites. Our data on Vav1 are similar to these observations, although we observe a maximum of only 4-fold rate enhancement. In the Vav1 acidic region, the tyrosines in the Y1 and Y3 motifs are separated by 32 residues while those in the Y2 and Y3 motifs are separated by only 14 residues. Both spacers are thus greater than the minimum required by Hck, but we only observe rate enhancement of Y3 upon initial phosphorylation at Y1 and not Y2. Although we do not have any direct evidence, it is likely that steric and/or orientational incompatibilities between SH2 docking to pY2 and Y3 substrate binding to the kinase active site could explain the observed differences between pY1 and pY2 interactions.

A model consistent with our NMR data, phosphorylation kinetics, and simulation results of the autoinhibited Y1-Y2-Y3-DH construct is shown in Figure 8b. As in the Y3-DH construct, the system exists in an equilibrium between open and closed states, where Y3 is accessible and inaccessible to kinases, respectively. In the longer construct both Y1 and Y2 motifs are unstructured and solvent exposed. Neither phosphorylation of these sites nor subsequent binding of SH2 domains to them alters the populations of open and closed states in the open−closed equilibrium (Figure 8b). However, the pY1 motif provides a docking site or "access point" for the Lck SH2 domain that effectively enhances affinity of the kinase for the protected Y3 motif. Interactions between Lck and this access point can alternatively be viewed as enabling the kinase to rapidly phosphorylate Y3 in intramolecular fashion.

In addition to the Ac and DH domains, Vav1 also contains several other modular domains that are important for proper regulation of activity. These likely act cooperatively with the Ac-DH element examined here. For instance, deletion of the Vav1 CH domain increases transforming activity of the protein, and cotransfection of constitutively active Lck with the truncated molecule further enhances this effect (*13*, *19*). Since transforming activity of Vav1 is coupled to its GEF activity, a simple explanation of these data is that the CH domain may also modulate Vav1 GEF activity. Several biochemical studies have also shown that the Vav1 CH domain can associate with either the DH domain or the CRD in vitro (*16*, *19*). These observations are further supported by the recent EM study of Vav3, where interactions between the CH domain and the CRD were observed in the full length protein that are disrupted upon phosphorylation (*21*). Therefore, the CH domain could further influence the conformational equilibrium in the core Y3-DH element and could cooperate to repress GEF activity and modulate kinase accessibility. In this light, how might the properties of the Y1-Y2-Y3-DH module investigated here relate to those of full length Vav1? The EM structure of Vav3 did not reveal whether Y1 and Y2 are exposed and unstructured in the full length protein as we observe in our minimal constructs here. If these motifs are disordered and exposed in the larger structure, then the kinetic properties we have observed here are likely preserved. If, however, the Ac domain interacts with other elements of full length protein, then Y1 and Y2 could be protected. In this case, it is not unreasonable that these interactions could be disrupted by phosphorylation, analogous to disruption of Y3-DH contacts upon phosphorylation of Tyr174. In such a scenario, the pY1 and pY2 constructs we have studied here could represent intermediates in the activation pathway of the full length protein. Their properties would then be operative in conversion of these intermediates to the fully active (i.e. pY3) molecule. These issues will be addressed in the future as part of our larger effort to understand the emergence of cooperativity in Vav1 through accretion of multiple individual domain−domain contacts.

Many autoinhibited proteins, including kinases (Src family kinases, twitchin kinases, Ca^{2+}/calmodulin-dependent kinases and PAK), GTPase effectors (WASP, MLK3, and mDia), and GTPase exchange factors (Vav, Dbl, Net1, Ost, Tiam, and Ect2), are being studied in great detail in an effort to understand how autoinhibition regulates function in this diverse group of molecules (*1*, *2*, *5*). In general, these proteins are all regulated by interactions between a regulatory domain and an activity bearing domain. Conformational dynamics are required for activation in all cases because the activator binding site on the regulatory domain partially overlaps with the autoinhibitory interface. In many examples where the structures are known, this overlap is not exact, however (*7*, *8*, *39*, *40*). We and others have suggested that the exposed regions of the regulatory domain may serve as initial contact sites (access points) for activators (*5*, *7*, *8*, *39*−*41*). While this construction is not necessary for relief of autoinhibition in all systems (see, for example the activation of Src by the phosphatase CD45 (*42*)), its widespread use suggests evolutionary pressure for the design. Access point contacts could facilitate relief of autoinhibition and enable the activator to better access the buried portion of the regulatory domain through a variety of mechanisms, such as changing the thermodynamics, kinetics, autoinhibitory contacts, or activator affinity. We have shown here that Vav1 can also function according to the access point model. However, in Vav1, the access points do not exist in the fully repressed wildtype protein. Therefore, the Src family kinases must first generate the access point through phosphorylation of an initial site, such as the Y1 motif in this study. Generation of an access point then allows kinase to dock through its SH2 domain leading to Vav1 activation. Therefore, sustained kinase activity may be required to generate access points, providing an additional level of control for Vav1 mediated signaling. Thus, variations of the general access point model, as described above, may allow for the general tuning of allosteric activation of autoinhibited proteins in response to different stimuli.

ACKNOWLEDGMENT

We thank Daisy Leung, Pilong Li, and Ilidio Martins for critical reading of the manuscript and numerous helpful discussions; Drs. Shae Padrick and Elliott Ross for helpful discussions; Chinatsu Otomo, Elisha White, and Junko Umetani for technical assistance; Dr. Eduardo Torres for the Lck SH32 construct; Dr. Kristen Lynch for providing laboratory space to conduct radioisotope studies; Bikash Pramanik and Dr. Haydn Ball for phosphopeptides and mass spectrometry analyses of phosphorylated Vav1 proteins; and members of the Rosen Lab for helpful suggestions and general assistance.

SUPPORTING INFORMATION AVAILABLE

Description of the DH domain protein constructs used in this study, schematic of reactions modeled in kinetic simulations of Vav1 phosphorylation, $^{1}H/^{13}C$ HSQC spectra, SDS−PAGE analyses, and representative raw kinetic data from the coupled phosphorylation assay. This material is available free of charge via the Internet at http://pubs.acs.org.

REFERENCES

1. Pufall, M. A., and Graves, B. J. (2002) Autoinhibitory domains: modular effectors of cellular regulation, *Annu. Rev. Cell Dev. Biol. 18*, 421−62.
2. Dueber, J. E., Yeh, B. J., Bhattacharyya, R. P., and Lim, W. A. (2004) Rewiring cell signaling: the logic and plasticity of eukaryotic protein circuitry, *Curr. Opin. Struct. Biol. 14*, 690−9.

3. Kobe, B., and Kemp, B. E. (1999) Active site-directed protein regulation, *Nature 402*, 373−6.
4. Kobe, B. (1999) Autoinhibition by an internal nuclear localization signal revealed by the crystal structure of mammalian importin alpha, *Nat. Struct. Biol. 6*, 388−97.
5. Huse, M., and Kuriyan, J. (2002) The conformational plasticity of protein kinases, *Cell 109*, 275−82.
6. Aghazadeh, B., Lowry, W. E., Huang, X. Y., and Rosen, M. K. (2000) Structural basis for relief of autoinhibition of the Dbl homology domain of proto-oncogene Vav by tyrosine phosphorylation, *Cell 102*, 625−33.
7. Goldberg, J., Nairn, A. C., and Kuriyan, J. (1996) Structural basis for the autoinhibition of calcium/calmodulin-dependent protein kinase I, *Cell 84*, 875−87.
8. Kim, A. S., Kakalis, L. T., Abdul-Manan, N., Liu, G. A., and Rosen, M. K. (2000) Autoinhibition and activation mechanisms of the Wiskott-Aldrich syndrome protein, *Nature 404*, 151−8.
9. Olson, M. F., Pasteris, N. G., Gorski, J. L., and Hall, A. (1996) Faciogenital dysplasia protein (FGD1) and Vav, two related proteins required for normal embryonic development, are upstream regulators of Rho GTPases, *Curr. Biol. 6*, 1628−33.
10. Mosteller, R., Han, J., Das, B., and Broek, D. (2000) Biochemical analysis of regulation of Vav, a guanine-nucleotide exchange factor for Rho family of GTPases, *Methods Enzymol. 325*, 38−51.
11. Bustelo, X. R. (2001) Vav proteins, adaptors and cell signaling, *Oncogene 20*, 6372−81.
12. Bustelo, X. R. (2002) Regulation of Vav proteins by intramolecular events, *Front. Biosci. 7*, d24−30.
13. Abe, K., Whitehead, I. P., O'Bryan, J. P., and Der, C. J. (1999) Involvement of NH(2)-terminal sequences in the negative regulation of Vav signaling and transforming activity, *J. Biol. Chem. 274*, 30410−8.
14. Abe, K., Rossman, K. L., Liu, B., Ritola, K. D., Chiang, D., Campbell, S. L., Burridge, K., and Der, C. J. (2000) Vav2 is an activator of Cdc42, Rac1, and RhoA, *J. Biol. Chem. 275*, 10141−9.
15. Crespo, P., Schuebel, K. E., Ostrom, A. A., Gutkind, J. S., and Bustelo, X. R. (1997) Phosphotyrosine-dependent activation of Rac-1 GDP/GTP exchange by the vav proto-oncogene product, *Nature 385*, 169−72.
16. Zugaza, J. L., Lopez-Lago, M. A., Caloca, M. J., Dosil, M., Movilla, N., and Bustelo, X. R. (2002) Structural determinants for the biological activity of Vav proteins, *J. Biol. Chem. 277*, 45377−92.
17. Han, J., Das, B., Wei, W., Van Aelst, L., Mosteller, R. D., Khosravi-Far, R., Westwick, J. K., Der, C. J., and Broek, D. (1997) Lck regulates Vav activation of members of the Rho family of GTPases, *Mol. Cell. Biol. 17*, 1346−53.
18. Bustelo, X. R., and Barbacid, M. (1992) Tyrosine phosphorylation of the vav proto-oncogene product in activated B cells, *Science 256*, 1196−9.
19. Lopez-Lago, M., Lee, H., Cruz, C., Movilla, N., and Bustelo, X. R. (2000) Tyrosine phosphorylation mediates both activation and downmodulation of the biological activity of Vav, *Mol. Cell. Biol. 20*, 1678−91.
20. Movilla, N., and Bustelo, X. R. (1999) Biological and regulatory properties of Vav-3, a new member of the Vav family of oncoproteins, *Mol. Cell. Biol. 19*, 7870−85.
21. Llorca, O., Arias-Palomo, E., Zugaza, J. L., and Bustelo, X. R. (2005) Global conformational rearrangements during the activation of the GDP/GTP exchange factor Vav3, *EMBO J. 24*, 1330−40.
22. Songyang, Z., and Cantley, L. C. (2004) ZIP codes for delivering SH2 domains, *Cell 116*, S41−3, 2 pp following S48.
23. Songyang, Z., Shoelson, S. E., Chaudhuri, M., Gish, G., Pawson, T., Haser, W. G., King, F., Roberts, T., Ratnofsky, S., Lechleider, R. J., et al. (1993) SH2 domains recognize specific phosphopeptide sequences, *Cell 72*, 767−78.
24. Margolis, B., Hu, P., Katzav, S., Li, W., Oliver, J. M., Ullrich, A., Weiss, A., and Schlessinger, J. (1992) Tyrosine phosphorylation of vav proto-oncogene product containing SH2 domain and transcription factor motifs, *Nature 356*, 71−4.
25. Kohno, T., Kusunoki, H., Sato, K., and Wakamatsu, K. (1998) A new general method for the biosynthesis of stable isotope-enriched peptides using a decahistidine-tagged ubiquitin fusion system: an application to the production of mastoparan-X uniformly enriched with 15N and 15N/13C, *J. Biomol. NMR 12*, 109−21.
26. Bradshaw, J. M., and Waksman, G. (1998) Calorimetric investigation of proton linkage by monitoring both the enthalpy and association constant of binding: application to the interaction of the Src SH2 domain with a high-affinity tyrosyl phosphopeptide, *Biochemistry 37*, 15400−7.
27. Delaglio, F., Grzesiek, S., Vuister, G. W., Zhu, G., Pfeifer, J., and Bax, A. (1995) NMRPipe: a multidimensional spectral processing system based on UNIX pipes, *J. Biomol. NMR 6*, 277−93.
28. Johnson, B. A. (2004) Using NMRView to visualize and analyze the NMR spectra of macromolecules, *Methods Mol. Biol. 278*, 313−52.
29. Barker, S. C., Kassel, D. B., Weigl, D., Huang, X., Luther, M. A., and Knight, W. B. (1995) Characterization of pp60c-src tyrosine kinase activities using a continuous assay: autoactivation of the enzyme is an intermolecular autophosphorylation process, *Biochemistry 34*, 14843−51.
30. Pellicena, P., Stowell, K. R., and Miller, W. T. (1998) Enhanced phosphorylation of Src family kinase substrates containing SH2 domain binding sites, *J. Biol. Chem. 273*, 15325−8.
31. Mendes, P. (1993) GEPASI: a software package for modelling the dynamics, steady states and control of biochemical and other systems, *Comput. Appl. Biosci. 9*, 563−71.
32. Turner, M., and Billadeau, D. D. (2002) VAV proteins as signal integrators for multi-subunit immune-recognition receptors, *Nat. Rev. Immunol. 2*, 476−86.
33. Hornstein, I., Alcover, A., and Katzav, S. (2004) Vav proteins, masters of the world of cytoskeleton organization, *Cell. Signalling 16*, 1−11.
34. Yaffe, M. B., Leparc, G. G., Lai, J., Obata, T., Volinia, S., and Cantley, L. C. (2001) A motif-based profile scanning approach for genome-wide prediction of signaling pathways, *Nat. Biotechnol. 19*, 348−53.
35. Lemmon, M. A., and Ladbury, J. E. (1994) Thermodynamic studies of tyrosyl-phosphopeptide binding to the SH2 domain of p56lck, *Biochemistry 33*, 5070−6.
36. Hubbard, S. R. (1997) Crystal structure of the activated insulin receptor tyrosine kinase in complex with peptide substrate and ATP analog, *EMBO J. 16*, 5572−81.
37. Yamaguchi, H., and Hendrickson, W. A. (1996) Structural basis for activation of human lymphocyte kinase Lck upon tyrosine phosphorylation, *Nature 384*, 484−9.
38. Hiromi, K. (1979) *Kinetics of Fast Enzyme Reactions: Theory and Practice*, John Wiley & Sons, New York.
39. Otomo, T., Otomo, C., Tomchick, D. R., Machius, M., and Rosen, M. K. (2005) Structural basis of Rho GTPase-mediated activation of the formin mDia1, *Mol. Cell 18*, 273−81.
40. Lei, M., Lu, W., Meng, W., Parrini, M. C., Eck, M. J., Mayer, B. J., and Harrison, S. C. (2000) Structure of PAK1 in an autoinhibited conformation reveals a multistage activation switch, *Cell 102*, 387−97.
41. Bi, F., Debreceni, B., Zhu, K., Salani, B., Eva, A., and Zheng, Y. (2001) Autoinhibition mechanism of proto-Dbl, *Mol. Cell. Biol. 21*, 1463−74.
42. Wang, D., Esselman, W. J., and Cole, P. A. (2002) Substrate conformational restriction and CD45-catalyzed dephosphorylation of tail tyrosine-phosphorylated Src protein, *J. Biol. Chem. 277*, 40428−33.

BI051126H